We are IntechOpen,
the world's leading publisher of
Open Access books
Built by scientists, for scientists

4,800
Open access books available

122,000
International authors and editors

135M
Downloads

154
Countries delivered to

Our authors are among the

TOP 1%
most cited scientists

12.2%
Contributors from top 500 universities

BOOK CITATION INDEX
CLARIVATE ANALYTICS
INDEXED

WEB OF SCIENCE™

Selection of our books indexed in the Book Citation Index
in Web of Science™ Core Collection (BKCI)

Interested in publishing with us?
Contact book.department@intechopen.com

Numbers displayed above are based on latest data collected.
For more information visit www.intechopen.com

2.5-D Time-Domain Finite-Difference Modelling of Teleseismic Body Waves

Hiroshi Takenaka[1] and Taro Okamoto[2]
[1]*Kyushu University*
[2]*Tokyo Institute of Technology*
Japan

1. Introduction

Teleseismic-waveform analysis is one of the most effective approaches for study of the earthquake source process. It is also useful for investigation of the subsurface structures since the teleseismic seismograms have much information on the structures beneath the stations as well as on those near source and around the paths between the source and the stations.

Analysing the teleseismic waveforms, we often calculate the synthetic seismograms. For complex structures such as subduction zones, however, it may be difficult to calculate accurate synthetic waveforms because of strong lateral heterogeneity. The laterally varying features such as steep sea-bottom topography and thick sedimentary layers can have a large effect even on long-period teleseismic body waveforms. For example, we can expect the large-amplitude later phases as the result of the structural effect, which cannot be predicted by the flat-layered model structure usually assumed in teleseismic-waveform analysis.

A full treatment of such effect requires a three-dimensional (3-D) model of the structure and a 3-D calculation for the wavefield, which requires 3-D numerical techniques such as the 3-D finite-difference or finite-element method. Recent advances in high performance computers have already brought full 3-D elastic modelling for seismic wave propagation within reach. Even a single CPU computer could now be used for full 3-D numerical simulations by exploitation of a single or multi-GPU (Graphics Processing Units) computing (e.g., Okamoto et al., 2010). However full 3-D modelling of large-scale seismic wave propagation is still computationally expensive due to its requirements for large memory and a large number of fast processors, and would be too costly even on parallel hardwares for solutions of large-sized problems in routine-like real data analyses because of many case computations. Nevertheless, in order to provide a quantitative analysis of real seismic records from complex regions such as subduction zones, we need to be able to calculate the 3-D wavefields.

An economical approach to modelling of seismic wave propagation which includes many important aspects of the propagation process is to examine the three-dimensional response of a model where the material parameters vary two-dimensionally. Such a configuration in which a 3-D field is calculated for a 2-D medium is sometimes called *two-and-a-half-dimensional* (2.5-D) problem (e.g., Eskola & Hongisto, 1981). As a compromise between realism and computational efficiency, 2.5-D methods for calculating 3-D wavefields in 2-D varying structures have been developed. Bleistein (1986) developed the ray-theoretical implications of

2.5-D modelling for acoustic problems. Luco et al. (1990) proposed a formulation for a 2.5-D indirect boundary method using Green's functions for a harmonic moving point force in order to obtain the 3-D response of an infinitely long canyon, in a layered half-space, for plane elastic waves impinging at an arbitrary angle with respect to the axis of the canyon. Pedersen et al. (1994) also presented a 2.5-D indirect boundary element method based on moving Green's functions to study 3-D scattering of plane elastic waves by 2-D topographies. Takenaka et al. (1996) have developed the 2.5-D discrete wavenumber–boundary integral equation method, coupled with a Green's function decomposition into P and S wave contributions, to consider the problem of the interaction of the seismic wavefield excited by a point source with 2-D irregular topography. Randall (1991) developed a 2.5-D velocity-stress finite-difference technique in time domain to calculate waveforms for multipole excitation of azimuthally nonsymmetric boreholes and formations. Okamoto (1994) also presented a 2.5-D finite-difference time-domain method, coupled with the reciprocal principle, to simulate the teleseismic records of a subduction earthquake. Furumura & Takenaka (1996) have developed an efficient 2.5-D formulation for the pseudospectral time-domain method for point source excitation and have applied this approach successfully to modelling the waveforms recorded in a refraction survey. Such 2.5-D methods can calculate 3-D wavefields without huge computer memory requirements, since they require storage only slightly larger than those of the corresponding 2-D calculations.

In this article we consider a 2.5-D elastodynamic equation in the time domain for obliquely incident plane waves as a means of modelling teleseismic wavefields for media with a 2-D variation in structure. For a 2-D medium, applying a spatial Fourier transform to the 3-D time-domain elastodynamic equation in the medium-constant direction along which the material parameters are constant, we get equations in the mixed coordinate-wavenumber domain. These can be solved as independent sets of 2-D equations for a set of wavenumbers. Okamoto (1994) solved the equations for each wavenumber by the staggered-grid finite-difference time-domain method and then applied an inverse Fourier transform over wavenumber (i.e. wavenumber summation) in order to obtain theoretical seismograms in the spatial domain. His time-domain approach solves the source-free elastodynamic equation in the time domain and needs to perform a large number of 2-D calculations. On the other hand, frequency-domain methods, such as the indirect boundary methods mentioned above, require only one 2-D calculation for solving plane-wave incidence problems; they do not require wavenumber summation because in 2.5-D plane-wave incidence problems the waveslowness (medium-constant directional component) is invariant, and so at each frequency the wavenumber (medium-constant directional component) is constant and equal to that of the incident wave. It may be related to the fact that arbitrary phase shift can easily be operated in the frequency domain while in the time domain the time shift operation is more difficult. Takenaka & Kennett (1996a) proposed a 2.5-D "time-domain" elastodynamic equation for plane-wave incidence, which does not require wavenumber summation. Takenaka & Okamoto (1997) then applied the staggered-grid finite-difference technique to this new 2.5-D equation for teleseismic body-waveform synthesis. It requires computation time only similar to the corresponding 2-D ones, and could reduce the computation time by nearly three order as compared to Okamoto (1994)'s method.

In the following sections of this article we describe the 2.5-D time-domain elastodynamic equation for plane-wave incidence and a staggered-grid finite-difference scheme for solving the equation, which do not require wavenumber summation, by following Takenaka &

Kennett (1996a;b) and Takenaka & Okamoto (1997). We then show two subjects of applications done by our group: one is an example of application to source-side structures, teleseismic waveform synthesis for source inversion; the other is an example of application to receiver-side structures, modelling for receiver function analysis.

2. 2.5-D elastodynamic equation for a plane-wave incidence

We first use the physical properties of the wavefield to derive a 2.5-D elastodynamic equation in the time domain for the situation of an incident plane wave. Throughout this article we employ a Cartesian coordinate system $[x, y, z]$, where the x and y are the horizontal coordinates and z is the vertical one.

For an isotropic linear elastic medium, the source-free 3-D elastodynamic equation in the time domain is given by

$$
\begin{aligned}
\rho \partial_{tt} u &= \partial_x \tau_{xx} + \partial_y \tau_{xy} + \partial_z \tau_{zx}, \\
\rho \partial_{tt} v &= \partial_x \tau_{xy} + \partial_y \tau_{yy} + \partial_z \tau_{yz}, \\
\rho \partial_{tt} w &= \partial_x \tau_{zx} + \partial_y \tau_{yz} + \partial_z \tau_{zz},
\end{aligned}
\tag{1}
$$

where $\rho = \rho(x, y, z)$ is the density, $[u, v, w] = \boldsymbol{u} = [u, v, w](x, y, z, t)$ are the displacements at a point (x, y, z) at time t, and the stress components are $\tau_{rs} = \tau_{rs}(x, y, z, t), (r, s = x, y, z)$. We have used a contracted notation for derivatives $\partial_{tt} \equiv \partial^2/\partial t^2$, and $\partial_r \equiv \partial/\partial r, (r = x, y, z)$. The stress and displacement components are related by the 3-D Hooke's law through the Lamé constants $\lambda = \lambda(x, y, z)$ and $\mu = \mu(x, y, z)$ as follows:

$$
\begin{aligned}
\tau_{xx} &= (\lambda + 2\mu)\partial_x u + \lambda(\partial_y v + \partial_z w), \quad \tau_{yy} = (\lambda + 2\mu)\partial_y v + \lambda(\partial_z w + \partial_x u), \\
\tau_{zz} &= (\lambda + 2\mu)\partial_z w + \lambda(\partial_x u + \partial_y v), \quad \tau_{yz} = \mu(\partial_z v + \partial_y w), \\
\tau_{zx} &= \mu(\partial_x w + \partial_z u), \qquad \tau_{xy} = \mu(\partial_y u + \partial_x v).
\end{aligned}
\tag{2}
$$

Numerical modelling schemes such as the finite-difference and pseudospectral methods can compute directly discretised versions of equations (1) and (2), where the bounded computational domains are usually represented by grids.

We now derive a 2.5-D equation of motion for a 3-D wavefield in a 2-D medium which is constant with respect to one coordinate and varies with the other two coordinates. We will assume the medium is constant in the y-direction throughout the rest of this article, so that the material properties take the form

$$
\lambda = \lambda(x, z), \quad \mu = \mu(x, z), \quad \rho = \rho(x, z).
\tag{3}
$$

Furthermore we assume the medium includes a homogeneous half-space underlying the 2-D heterogeneous region whose top may be bounded by a free surface.

Consider an upgoing plane wave with horizontal slowness $[p_x, p_y]$, which passes a point $[x_0, y_0, z_0]$ in the homogeneous half-space at a time $t = t_0$. The 3-D wavefield at arbitrary time and position in the medium including the 2-D heterogeneous region has the characteristic of repeating itself with a certain time delay for different observers along the medium-constant axis (i.e., y-axis). For instance, the wavefield in the vertical plane $y = y_0$ at the time $t = t_0$ must be identical to that in the vertical plane $y = 0$ at the time $t = t_0 - p_y y_0$. This means

$$
\boldsymbol{u}(x, y, x, t) = \boldsymbol{u}(x, 0, z, t - p_y y), \quad \tau_{rs}(x, y, x, t) = \tau_{rs}(x, 0, z, t - p_y y), \quad (r, s = x, y, z).
\tag{4}
$$

If the structure is invariant in both of the horizontal (x- and y-) directions so that the material properties depends only on the vertical (z-) direction (i.e., 1-D heterogeneous medium), equation (4) might reduce to

$$\boldsymbol{u}(x,y,x,t) = \boldsymbol{u}(0,0,z,t-p_x x - p_y y), \quad \tau_{rs}(x,y,x,t) = \tau_{rs}(0,0,z,t-p_x x - p_y y), \quad (r,s=x,y,z).$$
$$(5)$$

Note that this is 'Snell's law' for plane-wave propagation in a 1-D heterogeneous medium. Equation (4) is thus a *2.5-D version* of the 'Snell's law' which is also mentioned below. Equation (5) could be used for modelling three-component seismic plane waves in vertically heterogeneous media in the time domain (JafarGandomi & Takenaka, 2007; 2010; Tanaka & Takenaka, 2005).

Let us be back to the 2.5-D problem. From relations (4), the derivatives of the displacement and the stress with respect to y can be expressed as

$$\partial_y \boldsymbol{u}(x,y,x,t) = -p_y \partial_t \boldsymbol{u}(x,y,z,t), \quad \partial_y \tau_{rs}(x,y,x,t) = -p_y \partial_t \tau_{rs}(x,y,z,t), \quad (6)$$

where $\partial_t \equiv \partial/\partial t$. The equivalent relations for the stress in (4) and (6) can be derived directly from those for the displacement in (4) and (6) through equations (2) and (3).

Substituting (6) into (1) and (2) we obtain the equation of motion

$$\rho \partial_{tt} u = \partial_x \tau_{xx} - p_y \partial_t \tau_{xy} + \partial_z \tau_{zx},$$

$$\rho \partial_{tt} v = \partial_x \tau_{xy} - p_y \partial_t \tau_{yy} + \partial_z \tau_{yz}, \qquad (7)$$

$$\rho \partial_{tt} w = \partial_x \tau_{zx} - p_y \partial_t \tau_{yz} + \partial_z \tau_{zz},$$

and the stress representations

$$\tau_{xx} = (\lambda + 2\mu)\partial_x u + \lambda(-p_y \partial_t v + \partial_z w), \quad \tau_{yy} = -(\lambda + 2\mu)p_y \partial_t v + \lambda(\partial_z w + \partial_x u),$$

$$\tau_{zz} = (\lambda + 2\mu)\partial_z w + \lambda(\partial_x u - p_y \partial_t v), \quad \tau_{yz} = \mu(\partial_z v - p_y \partial_t w), \qquad (8)$$

$$\tau_{zx} = \mu(\partial_x w + \partial_z u), \qquad \tau_{xy} = \mu(-p_y \partial_t u + \partial_x v).$$

This set of equations represents the 2.5-D elastodynamic response of a medium in the absence of source. Note that all the variables in this set of equations are real-valued. When we solve equations (7) and (8), we can set $y = y_0$, so that these equations are reduced to 2-D ones. Once equations (7) and (8) have been solved for $y = y_0$, we can deduce the wavefield at any y from that at $y = y_0$ by shifting the time origin by $p_y(y - y_0)$ (see equation (4)).

We next give an alternative derivation of these time-domain 2.5-D equations (7) and (8), from the 2.5-D equations in the frequency-wavenumber domain, and recover the characteristic of the 2.5-D wavefield, equation (4), in the process of deriving these equations. Fourier-transforming the 3-D equations (1) and (2) with respect to t and y, we obtain the following source-free 2.5-D elastodynamic equation in the frequency-wavenumber domain:

$$-\omega^2 \rho \tilde{u} = \partial_x \tilde{\tau}_{xx} - ik_y \tilde{\tau}_{xy} + \partial_z \tilde{\tau}_{zx},$$

$$-\omega^2 \rho \tilde{v} = \partial_x \tilde{\tau}_{xy} - ik_y \tilde{\tau}_{yy} + \partial_z \tilde{\tau}_{yz}, \qquad (9)$$

$$-\omega^2 \rho \tilde{w} = \partial_x \tilde{\tau}_{zx} - ik_y \tilde{\tau}_{yz} + \partial_z \tilde{\tau}_{zz},$$

and stress-displacement relations:

$$\tilde{\tau}_{xx} = (\lambda + 2\mu)\partial_x\tilde{u} + \lambda(-ik_y\tilde{v} + \partial_z\tilde{w}), \quad \tilde{\tau}_{yy} = (\lambda + 2\mu)(-ik_y)\tilde{v} + \lambda(\partial_z\tilde{w} + \partial_x\tilde{u}),$$

$$\tilde{\tau}_{zz} = (\lambda + 2\mu)\partial_z\tilde{w} + \lambda(\partial_x\tilde{u} - ik_y\tilde{v}), \quad \tilde{\tau}_{yz} = \mu(\partial_z\tilde{v} - ik_y\tilde{w}), \tag{10}$$

$$\tilde{\tau}_{zx} = \mu(\partial_x\tilde{w} + \partial_z\tilde{u}), \qquad \tilde{\tau}_{xy} = \mu(-ik_y\tilde{u} + \partial_x\tilde{v}),$$

where we have used the y-invariance of the medium, i.e. equation (3), and have used the notation

$$\tilde{g}(x, k_y, z, \omega) = \frac{1}{2\pi}\int_{-\infty}^{\infty} dy\, e^{+ik_y y}\int_{-\infty}^{\infty} dt\, e^{-i\omega t} g(x, y, z, t), \tag{11}$$

for the transform to the frequency-wavenumber domain. For a fixed value of the wavenumber k_y, equations (9) and (10) depend on only two space coordinates, i.e. x and z. For each value of k_y, these equations can therefore be solved as independent 2-D equations. The invariance of the medium in the y direction means that there is no coupling between different k_y components. Whereas for full 3-D problems there would be coupling between different k_y wavenumber components. For 2.5-D problems with an incident plane wave, we need to consider only one k_y for each ω, which is that of the incident plane wave.

The inverse transform of the double Fourier transform (11) is

$$g(x, y, z, t) = \frac{1}{2\pi}\int_{-\infty}^{\infty} d\omega\, e^{+i\omega t}\int_{-\infty}^{\infty} dk_y\, e^{-ik_y y}\tilde{g}(x, k_y, z, \omega). \tag{12}$$

Changing the order of the integrations, and inserting the following relation between the wavenumber k_y and the slowness p_y:

$$k_y = \omega p_y, \tag{13}$$

equation (12) leads to

$$g(x, y, z, t) = \frac{1}{2\pi}\int_{-\infty}^{\infty} dp_y\int_{-\infty}^{\infty} d\omega\, e^{i\omega(t-p_y y)}|\omega|\tilde{g}(x, \omega p_y, z, \omega)$$

$$= \int_{-\infty}^{\infty} dp_y\, \hat{g}(x, p_y, z, t - p_y y), \tag{14}$$

where $\hat{g}$ in the time-slowness domain has been defined as

$$\hat{g}(x, p_y, z, t) \equiv \frac{1}{2\pi}\int_{-\infty}^{\infty} d\omega\, e^{i\omega t}|\omega|\tilde{g}(x, \omega p_y, z, \omega). \tag{15}$$

We then find

$$\frac{1}{2\pi}\int_{-\infty}^{\infty} d\omega\, e^{i\omega t}e^{-ik_y y}|\omega|\tilde{u}(x, k_y, z, \omega) = \hat{u}(x, p_y, z, t - p_y y), \tag{16}$$

and

$$\frac{1}{2\pi}\int_{-\infty}^{\infty} d\omega e^{i\omega t}e^{-ik_y y}ik_y|\omega|\tilde{u}(x, k_y, z, \omega) = p_y\partial_t\hat{u}(x, p_y, z, t - p_y y). \tag{17}$$

For an incident plane wave in a 2.5-D situation, the horizontal wavenumber k_y of all wavefields is constant for each ω, and equal to that of the incident plane wave. Further from (13) we require p_y to be invariant and equal to the y-component of the slowness of the incident

plane wave, which represents 'Snell's law' for 2.5-D problems as mentioned above. Thus, when the slowness of the incident wave is p_{y0}, $\hat{u}(x, p_y, z, t - p_y y)$ can be represented as

$$\hat{u}(x, p_y, z, t - p_y y) = \hat{u}(x, p_{y0}, z, t - p_{y0} y)\, \delta(p_y - p_{y0}), \tag{18}$$

where $\delta(x)$ is the Dirac delta function. Applying the inverse transform (12) to the displacement in the frequency-wavenumber domain $\tilde{u}(x, k_y, z, \omega)$, and using equations (14), (16) and (18), we obtain

$$u(x, y, z, t) = \hat{u}(x, p_{y0}, z, t - p_{y0} y). \tag{19}$$

Then,

$$\partial_t u(x, y, z, t) = \partial_t \hat{u}(x, p_{y0}, z, t - p_{y0} y). \tag{20}$$

We can recover (4) from (19) by appropriate substitutions: setting y to 0 we obtain an equation at time t and then making the particular choice $t - p_{y0} y$ gives

$$u(x, 0, z, t - p_{y0} y) = \hat{u}(x, p_{y0}, z, t - p_{y0} y) = u(x, y, z, t). \tag{21}$$

In a similar way, we can obtain the corresponding equation for the stress. Applying the partial Fourier inversions (16) and (17) to (9) and (10), and using equations (19) and (20), we recover the earlier forms (7) and (8).

In equations (7) and (8) the time derivatives appear on both sides of these equations, which may be inconvenient for direct discretisation with the finite-difference method. Here instead of direct use of equations (7) and (8), we employ the 2.5-D equation in terms of velocity-stress that is well suited to the use of the staggered-grid finite-difference technique. After some manipulation of (7) and (8) (Takenaka & Kennett, 1996b), we get the following velocity-stress formulation of the 2.5-D elastodynamic equation:

$$\partial_t \dot{u} = -p_y \rho_\beta^{-1} \mu \partial_x \dot{v} + \rho_\beta^{-1}(\partial_x \tau_{xx} + \partial_z \tau_{zx}),$$

$$\partial_t \dot{v} = -p_y \rho_\alpha^{-1} \lambda (\partial_x \dot{u} + \partial_z \dot{w}) + \rho_\alpha^{-1}(\partial_x \tau_{xy} + \partial_z \tau_{yz}),$$

$$\partial_t \dot{w} = -p_y \rho_\beta^{-1} \mu \partial_z \dot{v} + \rho_\beta^{-1}(\partial_x \tau_{zx} + \partial_z \tau_{zz}),$$

$$\partial_t \tau_{xx} = \nu \partial_x \dot{u} + \eta \partial_z \dot{w} - p_y \rho_\alpha^{-1} \lambda (\partial_x \tau_{xy} + \partial_z \tau_{yz}),$$

$$\partial_t \tau_{yy} = \rho_\alpha^{-1} \rho \lambda (\partial_x \dot{u} + \partial_z \dot{w}) - p_y \rho_\alpha^{-1}(\lambda + 2\mu)(\partial_x \tau_{xy} + \partial_z \tau_{yz}), \tag{22}$$

$$\partial_t \tau_{zz} = \eta \partial_x \dot{u} + \nu \partial_z \dot{w} - p_y \rho_\alpha^{-1} \lambda (\partial_x \tau_{xy} + \partial_z \tau_{yz}),$$

$$\partial_t \tau_{yz} = \rho_\beta^{-1} \rho \mu \partial_z \dot{v} - p_y \rho_\beta^{-1} \mu (\partial_x \tau_{zx} + \partial_z \tau_{zz}),$$

$$\partial_t \tau_{zx} = \mu (\partial_x \dot{w} + \partial_z \dot{u}),$$

$$\partial_t \tau_{xy} = \rho_\beta^{-1} \rho \mu \partial_x \dot{v} - p_y \rho_\beta^{-1} \mu (\partial_x \tau_{xx} + \partial_z \tau_{zx}),$$

where $[\dot{u}, \dot{v}, \dot{w}] = [\dot{u}, \dot{v}, \dot{w}](x, y, z, t)$ is the particle velocity, and

$$\rho_\alpha \equiv \rho - p_y^2 (\lambda + 2\mu) = \rho(1 - \alpha^2 p_y^2),$$

$$\rho_\beta \equiv \rho - p_y^2 \mu = \rho(1 - \beta^2 p_y^2), \tag{23}$$

$$\nu \equiv (\lambda + 2\mu) + p_y^2 \rho_\alpha^{-1} \lambda^2, \quad \eta \equiv \lambda + p_y^2 \rho_\alpha^{-1} \lambda^2,$$

with P-wave velocity α and S-wave velocity β. When we solve (22), we can set $y = 0$ as well as the case of (7) and (8) .

3. Finite-difference scheme

We use a staggered-grid finite-difference scheme (e.g., Hayashida et al., 1999; Levander, 1988; Virieux, 1986), which is stable for any values of Poisson's ratio, making it ideal for modelling marine problems. The finite-difference grid is staggered in time and two-dimensional space (x-z plane) as shown in Fig. 1. The y-components of particle velocity $\hat{v}$ locates at the same grid points as the normal stresses both in time and space. We should note the y coordinate is not discretised but continuous. Letting $x = i\Delta x$ or $x = (i \pm 1/2)\Delta x$, $z = j\Delta z$ or $z = (j \pm 1/2)\Delta z$, and $t = l\Delta t$ or $t = (l \pm 1/2)\Delta t$; Δx and Δz are the grid spacings in the x- and z-direction, respectively, and Δt is the time step, and using Levander's notation (Levander, 1988), the difference equations for (22) are, for example,

$$
\begin{aligned}
D_t^+ \dot{u}(i, j+1/2, l) = {} & \rho_\beta^{-1}(i, j+1/2) \times \\
& [-p_y \mu(i, j+1/2) D_x^- \hat{v}(i+1/2, j+1/2, l+1/2) \\
& + D_x^- \tau_{xx}(i+1/2, j+1/2, l+1/2) + D_z^+ \tau_{zx}(i, j, l+1/2)],
\end{aligned}
$$

$$
\begin{aligned}
D_t^+ \tau_{xx}(i+1/2, j+1/2, l+1/2) = {} & \nu(i+1/2, j+1/2) D_x^+ \dot{u}(i, j+1/2, l+1) \qquad (24)\\
& + \eta(i+1/2, j+1/2) D_z^+ \dot{w}(i+1/2, j, l+1) \\
& - p_y \rho_\alpha^{-1}(i+1/2, j+1/2) \lambda(i+1/2, j+1/2) \times \\
& [D_x^+ \tau_{xy}(i, j+1/2, l+1) + D_z^+ \tau_{yz}(i+1/2, j, l+1)],
\end{aligned}
$$

where D_t^+ is forward difference operator in time, and $D_x^\pm$ and $D_z^\pm$ are the forward- or backward-difference operators in space, with sign chosen to center the difference operator about the quantity being updated. For example, in case of a second-order accurate in time and fourth-order accurate in space scheme we used,

$$
D_t^+ \dot{u}(i, j+1/2, l) = \frac{1}{\Delta t}[\dot{u}(i, j+1/2, l+1) - \dot{u}(i, j+1/2, l)],
$$

$$
\begin{aligned}
D_x^- \hat{v}(i+1/2, j+1/2, l+1/2) = {} & \frac{1}{\Delta x}\{c_1[\hat{v}(i+1/2, j+1/2, l+1/2) - \hat{v}(i-1/2, j+1/2, l+1/2)] \\
& - c_2[\hat{v}(i+3/2, j+1/2, l+1/2) - \hat{v}(i-3/2, j+1/2, l+1/2)]\},
\end{aligned}
$$

$$
\begin{aligned}
D_z^+ \tau_{zx}(i, j, l+1/2) = {} & \frac{1}{\Delta z}\{c_1[\tau_{zx}(i, j+1, l+1/2) - \tau_{zx}(i, j, l+1/2)] \qquad (25)\\
& - c_2[\tau_{zx}(i, j+2, l+1/2) - \tau_{zx}(i, j-1, l+1/2)]\},
\end{aligned}
$$

where $c_1 = 9/8$, $c_2 = 1/24$.

The fourth-order spatial finite-difference scheme usually needs more than five grid points per wavelength (Levander, 1988). The finite-difference region (computational domain) is divided into two parts: a *model zone* for the upper part and an *initial wave zone* for the lower part. The model zone fully includes the target structural model and may be heterogeneous. The initial wave zone locates under the model zone and should be homogeneous. It is needed for the incident wave, and an upgoing plane wave is input as the initial condition within it. The initial wave zone should have no velocity contrast at the interface contacting the model zone

to prevent artificial reflections and conversions. The size of the computational domain is set sufficiently large so that artificial noises, such as noises from the both ends of the input plane wave, can be ignored. As Okamoto (1994) we here select the time step as 62 % of the maximum allowed time step by the stability condition for the 2-D $P - SV$ finite-difference scheme of a second-order accurate in time and fourth-order accurate in space (Levander, 1988).
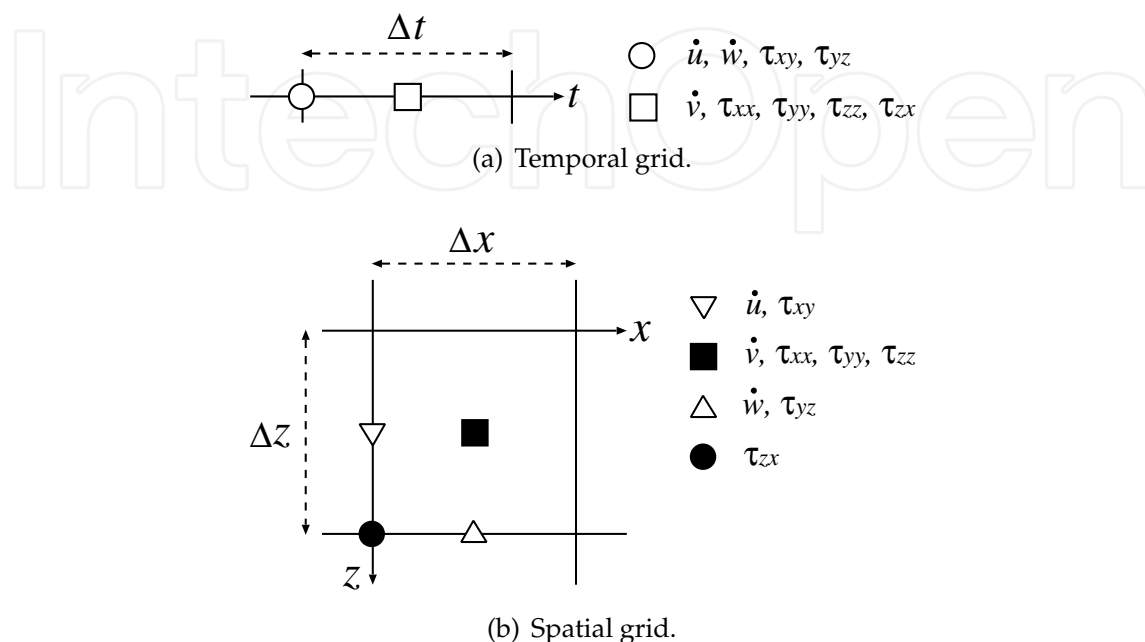

(a) Temporal grid.

(b) Spatial grid.

Fig. 1. Discretisation of (a) time and (b) space.

4. Teleseismic waveform synthesis for source inversion

Seismic displacement due to a point source of earthquake may be expressed as

$$u_n(x,t) = M_{pq}(t) * \partial_q G_{n;p}(x,t;\xi,0), \tag{26}$$

where $M_{pq}(t)$ is moment tensor with time varying components, operation $*$ is convolution with respect to time t, and $G_{n;p}(x,t;\xi,\tau)$ is displacement Green's tensor representing the nth component of elastic displacement at a receiver position x and time t caused by a unit point force in the p-direction at a source position ξ and time τ (e.g., Aki & Richards, 2002). We have used the convention of summation over repeated suffices. In source inversions derivative of the GreenÅfs tensor $\partial_q G_{n;p}(x,t;\xi,0)$ is empirically called just "Green's function". We here follow this custom.

Applying the spatial reciprocity:

$$G_{n;p}(x,t;\xi,0) = G_{p;n}(\xi,t;x,0), \tag{27}$$

equation (26) reduces to

$$\begin{aligned} u_n(x,t) &= M_{pq}(t) * \partial_q G_{p;n}(\xi,t;x,0) \\ &= M_{pq}(t) * E_{pq;n}(\xi,t;x,0), \end{aligned} \tag{28}$$

where $E_{pq;n}(\xi,t;x,0)$ is the strain tensor at the source position corresponding to $G_{p;n}(\xi,t;x,0)$. This equation shows as follows. The reciprocity of the elastodynamic theory is exploited

to calculate the Green's functions. The displacement at receiver due to the moment tensor at source can be calculated by solving the reciprocal problem; the reciprocal relation is applied to the response displacement at the source position due to a unit body force acting at the receiver position. In the teleseismic problem, the virtual force is applied at infinity (i.e., station location). Since we are only concerned with the teleseismic body waves, the wavefield due to this virtual force can be approximated by a plane wave. The response of the near-source structure to an incident plane wave is then calculated and converted to the far-field displacement. This approach using the reciprocity for teleseisimic body wave synthesis was employed by Bouchon (1976) where a simple method was presented, which combines the reciprocity theorem and the flat layer theory (Thomson-Haskell matrix formulation: Haskell, 1953; Thomson, 1950) to yield teleseismic body wave radiation from seismic sources embedded in the horizontally layered crustal models.

For the conversion to the far-field displacement, based on the assumption of ray propagation in the mantle, the response of the near-source structure mentioned above is multiplied by the geometrical spreading effect within the mantle upon the amplitude of the body wave and convolution with the source time function, with atenuation operator for the path in the mantle, with the response at the surface of the receiver crust for the incident impulsive teleseismic body wave, and with the instrumental response, where the actually employed response of the receiver crust often accounts for only the free surface effect at the receiver or is calculated from a very simple crustal model (this issue may be related to the subject of the next subsection). This method has been extensively used to calculate teleseismic waveforms for studies on earthquake source processes (e.g., Miyamura & Sasatani, 1986). Even now it is one of the most popular methods for calculation of teleseismic Green's functions in routine-like source inversions (e.g., Kikuchi & Kanamori, 1991; Nakamura et al., 2009).

The reciprocal formulation has the following advantages: for a single station the Green's functions for many point sources at different positions can be obtained simultaneously in a single numerical calculation, which facilitates the waveform analysis to find the best position for the earthquake source location without repeating the time-consuming numerical calculations. Although Bouchon (1976) actually treated calculation for horizontally layered structures, he mentioned in the paper that the reciprocal approach is also applicable to the case of a source in a layered structure with irregular interfaces. Wiens (1987; 1989) and Yoshida (1992) applied this approach to planar-dipping structures including the sea floor by using a ray-theoretical technique developed by Langston (1977). Furthermore Okamoto & Miyatake (1989) and Okamoto (1993) extended it to arbitrary 2-D heterogeneous structures by using the finite-difference method in time domain. However, their calculation is based on the 2-D elastodynamic equation, and is limited to two dimenions, so that the available stations are restricted to those located in the direction perpendicular to the medium-constant axis (y-axis in the previous sections). This restriction in the azimuthal coverage makes it difficult to examine the source process in detail.

In order to get teleseismic synthetics for arbitrary azimuth Okamoto (1994) proposed a method for calculating the 2.5-D telseismic body waves, which solves the time-domain version of 3-D elastodynamic equation in the mixed coordinate (x and z)-wavenumber (k_y) domain (9) and (10) for each of a number of discretised wavenumber k_y with the finite-difference time-domain scheme and perform an inverse Fourier transform over wavenumber k_y (i.e. wavenumber summation) to obtain the synthetic seismograms in the spatial domain. His method requires the computation time more than hundreds times of the corresponding 2-D computations.

Takenaka et al. (1997) presented a method without wavenumber summation so that 2.5-D teleseismic synthetics requires only computation time similar to the corresponding 2-D ones. This method uses the 2.5-D elastodynamic equation for a plane-wave incidence (22) and its finite-difference time-domain scheme proposed by Takenaka & Okamoto (1997) which was described in the previous section. It has been employed for calculating teleseismic Green's functions in several source inversion studies (e.g., Okamoto & Takenaka, 2009a;b) and for modelling the teleseismic waveforms including a near-source scattering inside a subducted plate (Kaneshima et al., 2007). We here show two results for source inversion among them as examples.

Figure 2 shows comparison of the teleseismic Green's function waveforms from the 2-D model with those from 1-D (flat-layered) models for a source inversion of the 17-July-2006 Java tsunami earthquake (M_W7.8 by Okamoto & Takenaka, 2009a, USGS PDE: 08:19:26.6, 9.284°S, 107.419°E, depth 20 km, http://earthquake.usgs.gov/research/data). The material properties of the assumed Java trench model (Fig. 2(a)) are allowed to vary with respect to the trench-perpendicular axis, while they are assumed to be invariant with respect to the trench-parallel axis. This model was constructed from the results of seismic surveys in the nearby area (Kopp et al., 2002) and global reference models (Dziewonski & Anderson, 1981; Kennett & Engdahl, 1991; Laske et al., 2001). In Fig. 2(a) the point sources for Green's function computations are located along the dip of the main-shock fault plane. The along-dip interval of source points is 8.0 km for the section from S1 to S8 and 8.1 km for the section from S8 to S15. The rigidity for sources S1-S7 is 16.3 GPa and for sources S8-S15, 38.6 GPa. The best double couple of the Global CMT solution (http://www.globalcmt.org) shown in Fig. 2(b) is employed for each Green's function computation. Following the standard 1-D teleseismic wave computations, mantle attenuation is incorporated by choosing $t^* = 1.0$ for P-waves and 4.0 for SH-waves, while anelastic attenuation is not included in the finite-difference computations that evaluate near-source response. The 1-D Green's functions were computed by the method of Kroeger & Geller (1983). The comparison between waveforms of the 2.5-D and flat-layered Green's functions (Fig. 2(c)) clearly illustrates the large effect of the heterogeneous structure on the body waves. The waveforms of 2.5-D Green's functions have prolonged, large amplitude later phases. They appear irrespective of station azimuth, and are not reproduced by 1-D model. At the oceanic trench regions large effect of laterally heterogeneous structure is expected to appear on the teleseismic body waveforms: thick water layer, dipping ocean bottom, and thick sediments near the source distort ray paths to teleseismic stations and often cause large later phases on the teleseismic body waveforms. This effect must be evaluated carefully before a detailed source process analysis is applied to real earthquake records.

Okamoto & Takenaka (2009b) studied strong effect of near-source structure on teleseismic body waveforms from two well-recorded aftershocks of the 2006 Java tsunami earthquake. Figure 3 shows the results of one of the two events: M_W6.1, 2006/07/17 15:45:59.8, 9.420°S 108.319°E. They applied a "waveform relocation technique" which combines a waveform inversion of source parameters with a grid search procedure to correct possible systematic bias in hypocentral parameters. In the waveform inversion 2.5-D teleseismic Green's functions are used. The grid spacing for grid search is 2 km horizontally and 1 km vertically. In Fig. 3(b), the 2.5-D synthetic seismograms are compared with the observation records. In most of the stations, peaks and troughs in the observed later arrivals are well reproduced by the synthetics. The best position (Fig. 3(a), (c)) and the mechanism (Fig. 3(b)) of the obtained point
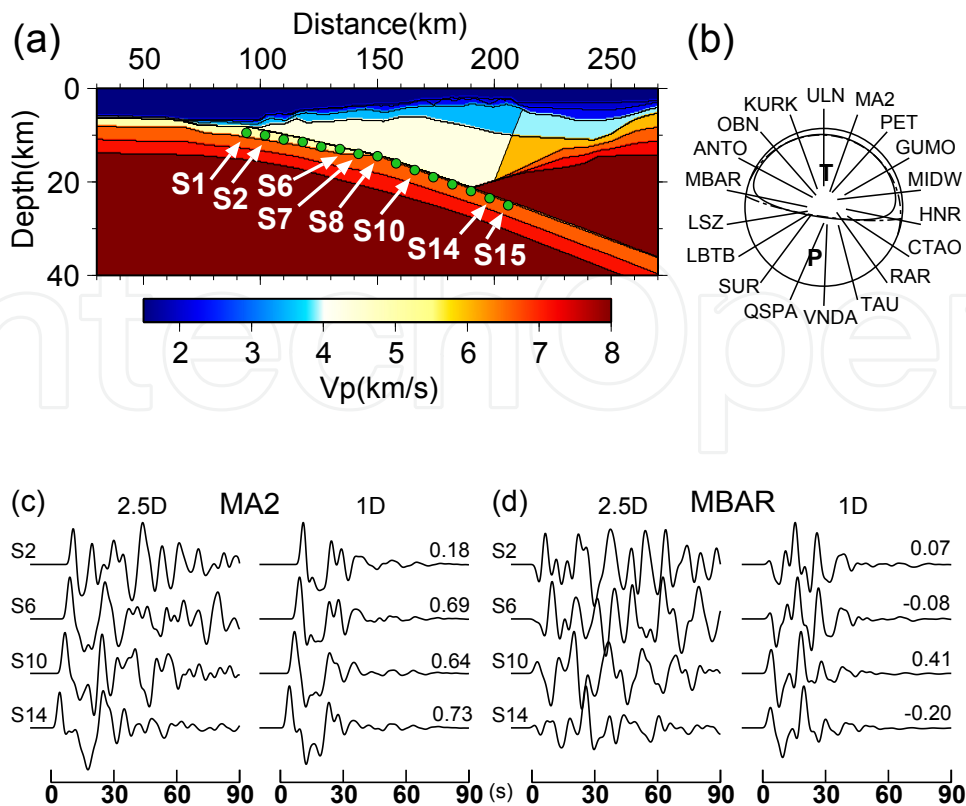
Fig. 2. (a) 2-D model of the Java trench. *P*-wave velocity is shown in colour scale (*S*-wave velocity is zero in the ocean). Green circles denote point source positions along the dip for Green's function computations. (b) Global CMT solution of the main shock and the teleseismic station coverage. (c) Examples of synthetic *P*-waveforms (Green's functions) for station MA2. 2.5D denotes those computed for the 2-D model of the near-source structure, and 1D denotes those for the flat-layered model. Attached indexes (S2-S14) denote the source positions. Numbers attached to the 1-D waveforms denote cross-correlation coefficients between 1-D and corresponding 2.5-D Green's functions for a dulation from 0 to 90 s. The 1-D model consists of a standard crust (Kennett & Engdahl, 1991) additionally overlain by a 3-km-thick ocean and 2-km-thick sediment. (d) Same as (c) but for station MBAR. (Reproduced from Okamoto & Takenaka, 2009a).

source are close to those of the Global CMT. The residual contour distribution in Fig. 3(a) and the RMS error plots in Fig. 3(c) indicate that the source location could be well constrained both vertically and horizontally. Use of the 2.5-D modelling makes it possible to obtain improved source parameters at the trench regions where only teleseismic data are available.

5. Modelling for receiver function analysis

Receiver function analysis is one of the effective and popular methods for study of the crust and upper mantle structures using teleseismic waveform data (e.g., Ammon, 1991; Cassidy, 1992; Dugda et al., 2005; Farra & Vinnik, 2000; Kanao & Shibutani, 2011; Langston, 1979; Owens et al., 1988; Saita et al., 2002; Suetsugu et al., 2004; Zhu & Kanamori, 2000). In the analysis it is often necessary to calculate synthetic waveforms for the structure models. For this purpose horizontally layered structure models have been assumed, because the response
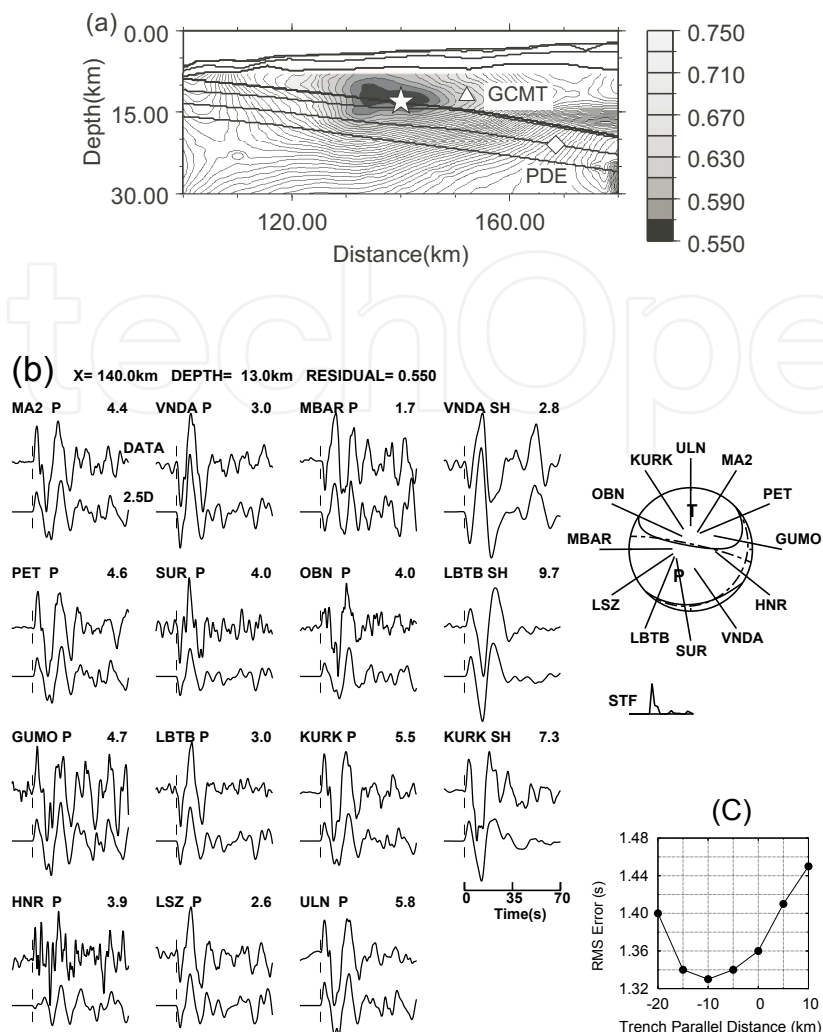
Fig. 3. (a) Open star indicates the best point source position of the 17-July-2006 event (M_W6.1). Locations of Global CMT (triangle) and PDE (diamond) are also projected. The contour lines denote the residual distribution of the grid search relocation by the waveform inversion. The contour interval is 0.02. (b) Observed (top) and 2.5-D synthetic (bottom) waveforms. Attached number denotes the maximum amplitude of the observed waveform in μm. Also plotted are the source time function (STF) and the focal mechanism. A time window of 70 s after the onset (indicated by vertical lines) is used for the inversion. The estimated moment tensor components in unit of 10^{17} Nm are: $M_{rr} = -1.81$, $M_{\theta\theta} = 4.63$, $M_{\phi\phi} = -2.81$, $M_{r\theta} = 11.1$, $M_{r\phi} = -2.04$, $M_{\theta\phi} = 0.67$, which yield a scalar moment of 1.19×10^{18} Nm (M_W6.0). (c) RMS error in travel time analysis plotted versus the distance with respect to trench-parallel axis (positive toward N116°E with the origin placed on the cross section through the PDE epicenter). Most of the travel times listed in USGS NEIC Monthly Earthquake Data Report are used. (Reproduced from "Effect of near-source trench structure on teleseismic body waveforms: an application of a 2.5D FDM to the Java trench" by T. Okamoto & H. Takenaka, in *Advances in Geosciences*, Vol. 13 (Solid Earth), Ed. Kenji Satake, Copyright (C) 2009 by World Scientific Publishing.)

of such a simple structure model to teleseismic P wave (plane wave) can be calculated easily and accurately by a semi-analytical method such as the Thomson-Haskell matrix method (Haskell, 1953; Thomson, 1950). However, for structures with strong lateral heterogeneity such as subdunction zones, it is often difficult to consider horizontally layered media for modelling the teleseismic body waves that propagate through such complex structures. Full 3-D modelling of seismic wave propagation is still computationally intensive. Takenaka & Okamoto (1997) used the 2.5-D finite-difference method described in the previous sections to simulate teleseismic seismograms at ocean-bottom stations for assessing the effect of sea-bottom topography. Ando et al. (2003) applied this approach to a profile across a realistic model of subduction zone structure to simulate the effect of a subducting slab on the receiver function waveforms observed at subduction zone, and Takenaka et al. (2004) then clearly demonstrated the azimuthal dependence of the slab-converted phases in the receiver functions. We here illustrate their results.
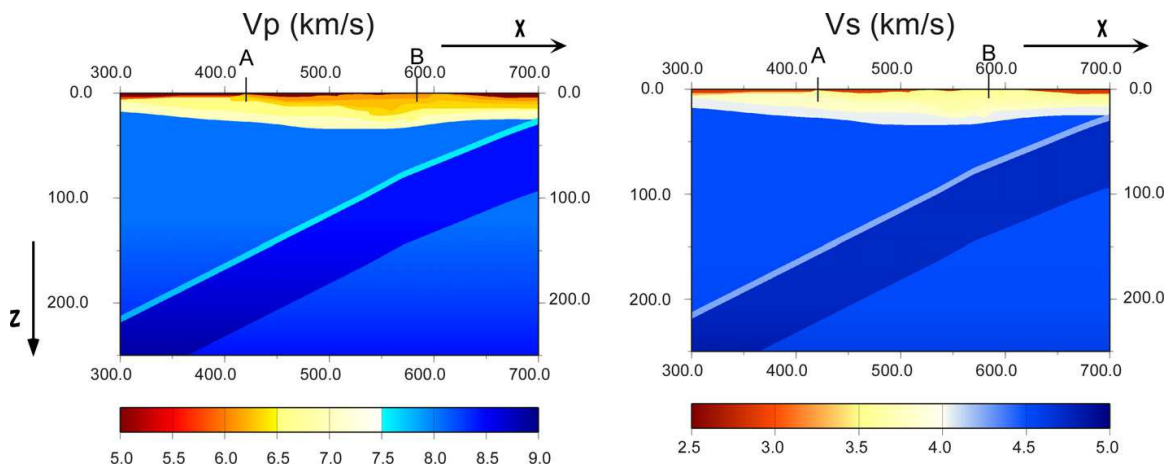
Fig. 4. P- and S-wave velocity profiles of a subduction zone model. The slab consists of two layers: the upper layer of 7 km thickness corresponding to the oceanic crust has velocities of 6 % lower relative to the mantle of the ak135 model (Kennett et al., 1995), while the lower layer corresponding to the oceanic slab mantle has velocities of 5 % higher relative to the ak135 mantle.
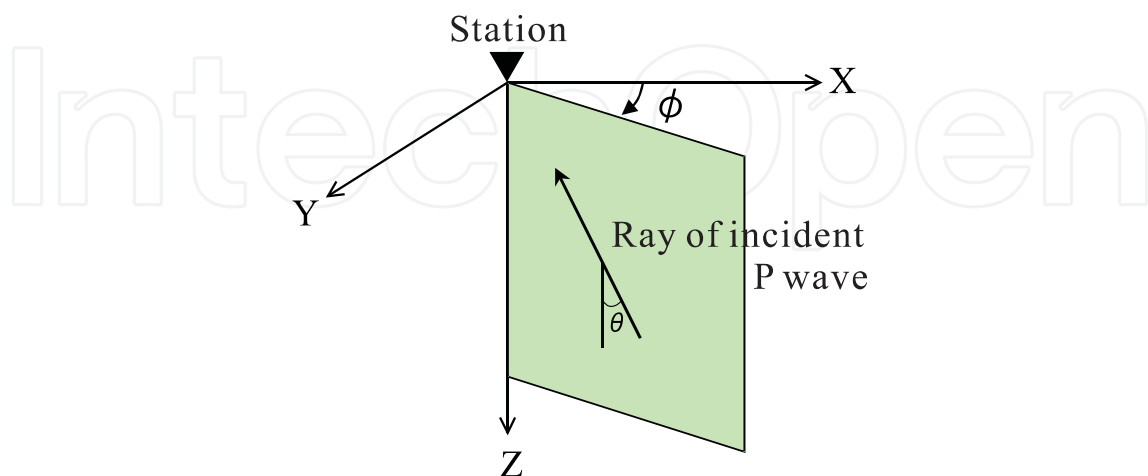
Fig. 5. Geometrical definitions. θ is the incident angle of a plane P wave, and ϕ is the backazimuth.

Figure 4 shows a cross-section of a subduction zone model which is an analogue to that of Tohoku, Japan. The shown area is the target where all the seismic phases for the receiver functions are modelled. The actual computational domain is set sufficiently larger so that artificial reflection noises from the bottom and both sides of the domain do not contaminate the synthetic seismograms. The synthetic seismograms of teleseismic P wave at the ground surface between A and B in Fig. 4 were calculated for events of epicentral distance $80°$ with backazimuths of $0°$ to $180°$ in the interval of $22.5°$. The definition of the backazimuth (ϕ) is indicated in Fig. 5. The epicentral distance $80°$ corresponds to the P-wave incident angle of around $17°$ at the surface. Three-components of the synthetic seismograms for the teleseismic events of backazimuths of $0°$ and $90°$ are shown in Fig. 6. The signal of the incident wave (source wavelet) was assumed to be a simple Gaussian pulse. The radial and transverse receiver functions for each backazimuth event can be calculated from the synthetic seismograms (Fig. 7).
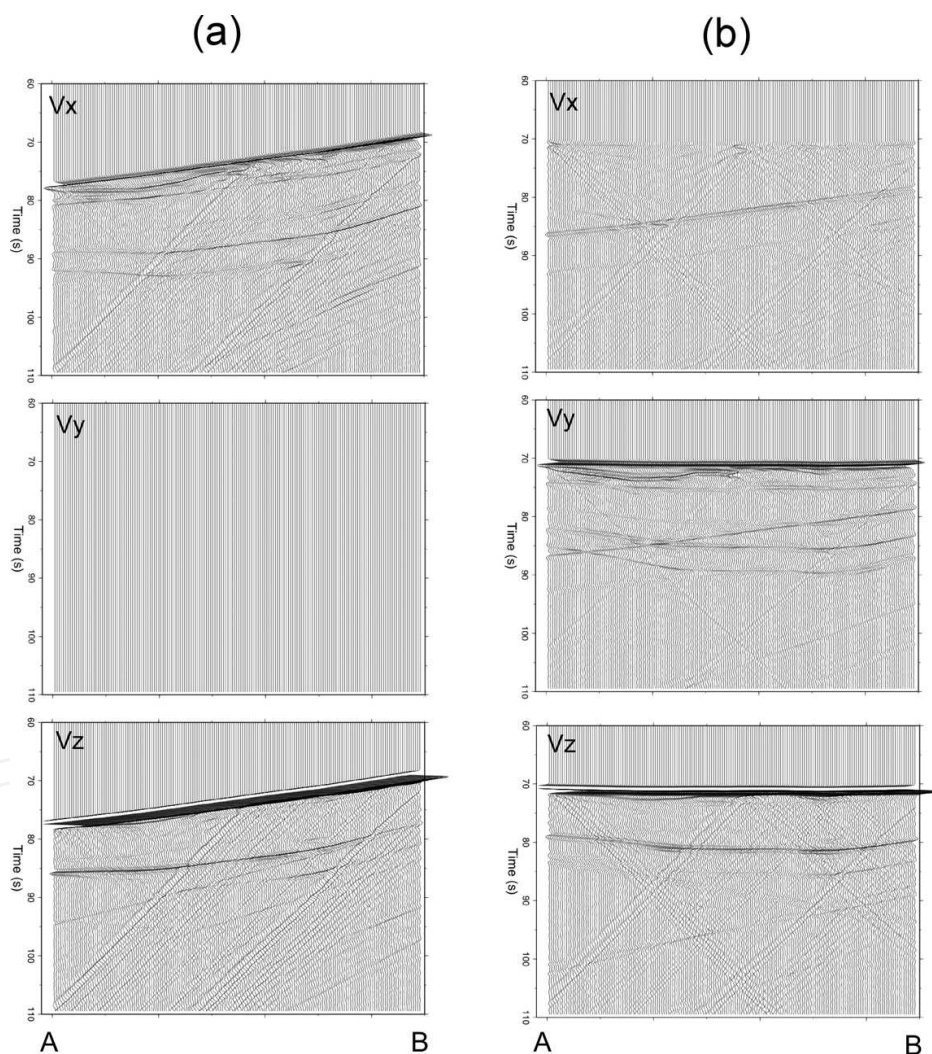
Fig. 6. Examples of three-component waveforms for events of (a) $\phi = 0°$ and (b) $\phi = 90°$. V_x, V_y, and V_z are the x-, y-, and z-components, respectively.

Figure 8(a) displays circular plots of the radial receiver functions over backazimuth of events for three stations. The receiver functions for backazimuths of more than $180°$ can be obtained from the synthetic seismograms for backazimuths of less than $180°$ through symmetrical
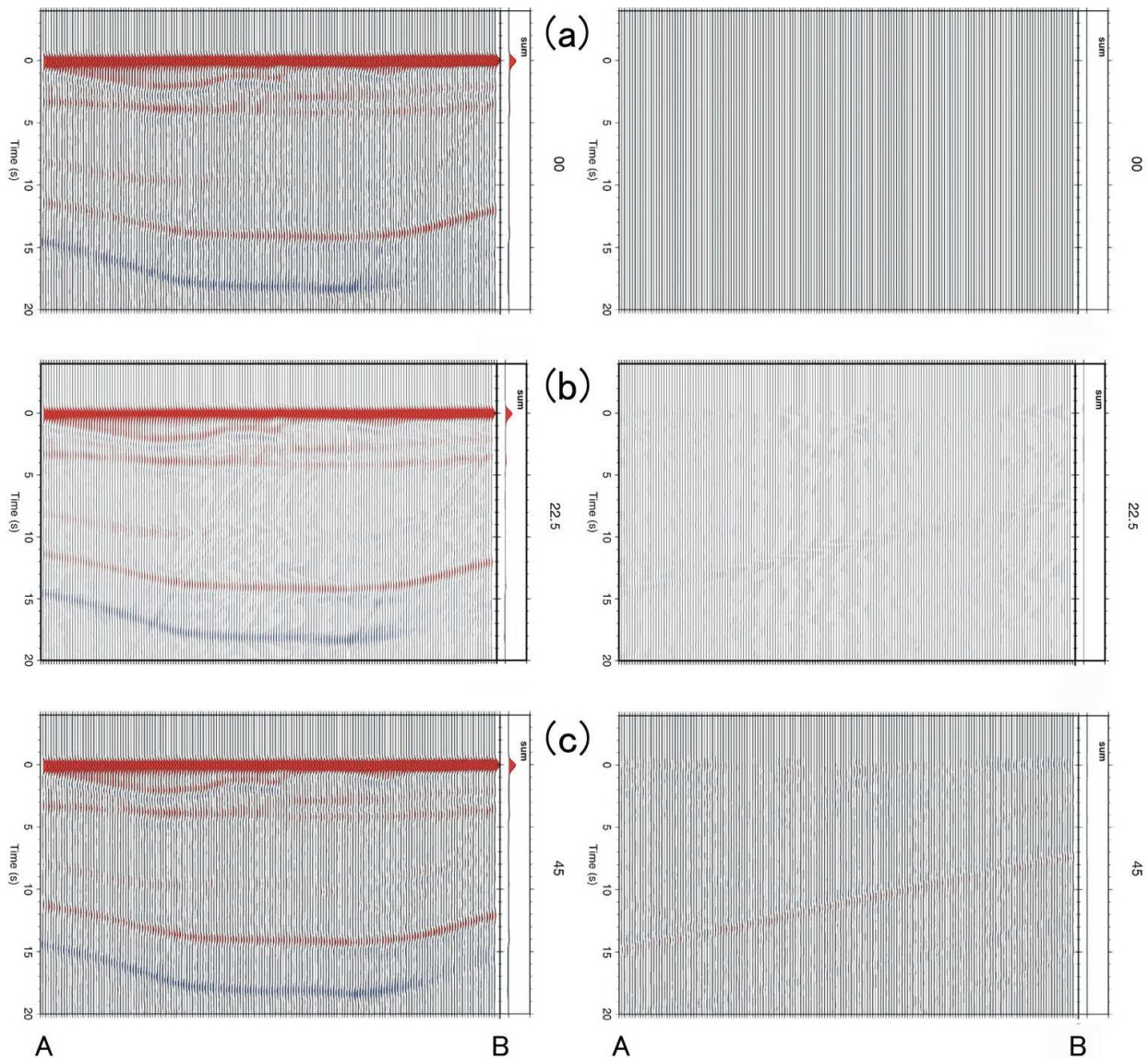
Fig. 7. Receiver function profiles between A and B at the surface (see Fig. 4) for nine teleseismic events of (a) $\phi = 0°$, (b) $\phi = 22.5°$, (c) $\phi = 45°$, (d) $\phi = 67.5°$, (e) $\phi = 90°$, (f) $\phi = 112.5°$, (g) $\phi = 135°$, (h) $\phi = 157.5°$, and (i) $\phi = 180°$. Left column: radial receiver functions. Right column: transverse receiver functions. Red and blue colours are positive and negative amplitudes, respectively. The Gaussian filter $G(\omega) = \exp[-\omega^2/(4a^2)]$ of $a = 2.5$ has been applied to all receiver functions.

properties of seismic wavefields with respect to the azimuth of the incident plane wave. Figure 8(b) shows linear plots of the radial and transverse receiver functions for the left station among the three stations shown in Fig. 8(a). In both components of the receiver functions the slab Ps phases generated at dipping interfaces are clearly seen as convex arrival patterns with the latest arrival around 17 s at backazimuth of $180°$. The slab-converted phases exhibit the amplitude and arrival-time variations as a function of the backazimuth: the arrival is the latest for the backazimuth (ϕ) which is equal to the dip direction of the slab ($\phi_0 = 180°$); and the amplitude variation shows a pattern with the backazimuth like $\cos[(\phi - \phi_0)/2]$ for the radial receiver function, and $\cos(\phi - \phi_0)$ for the transverse one, respectively.
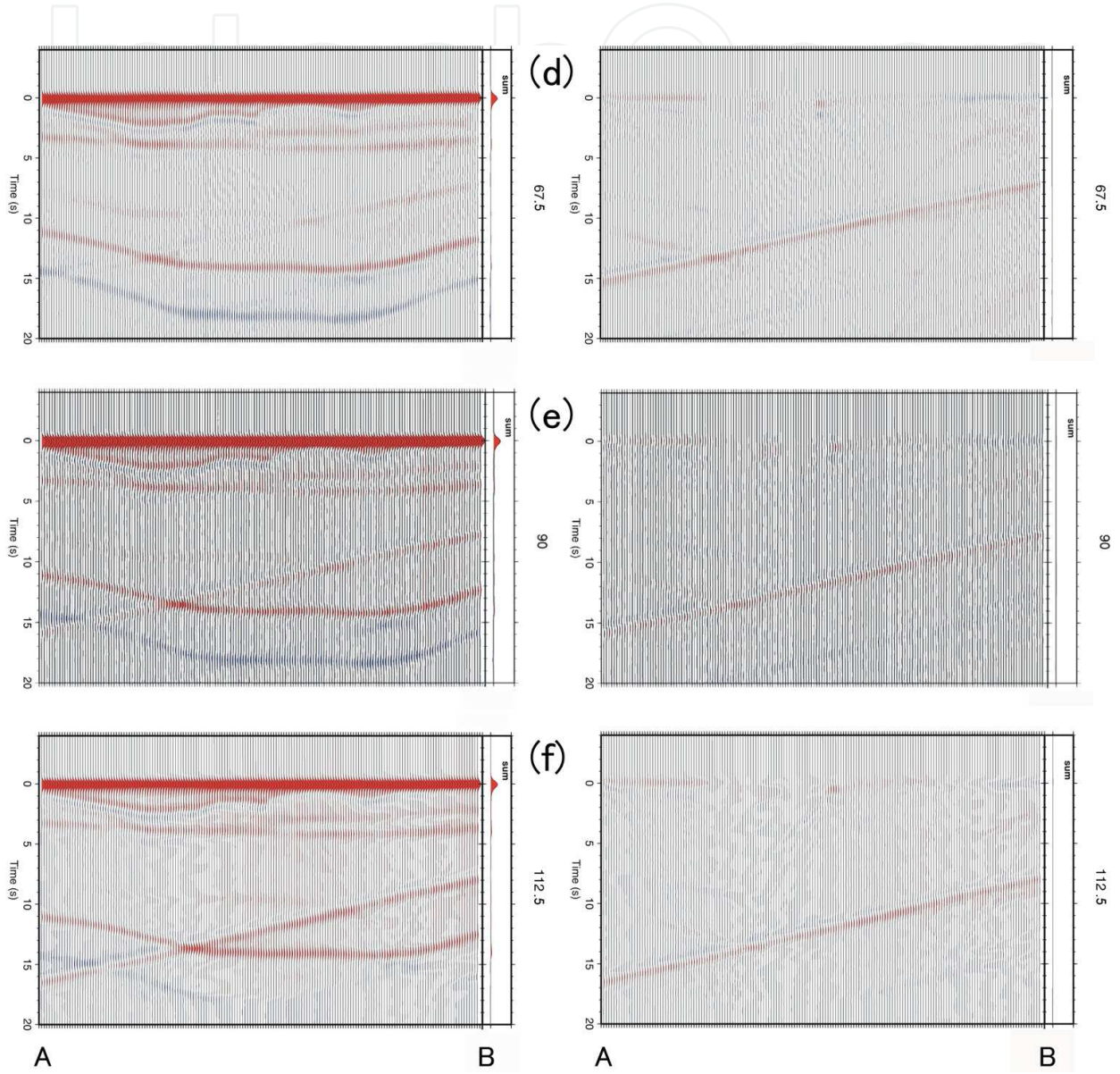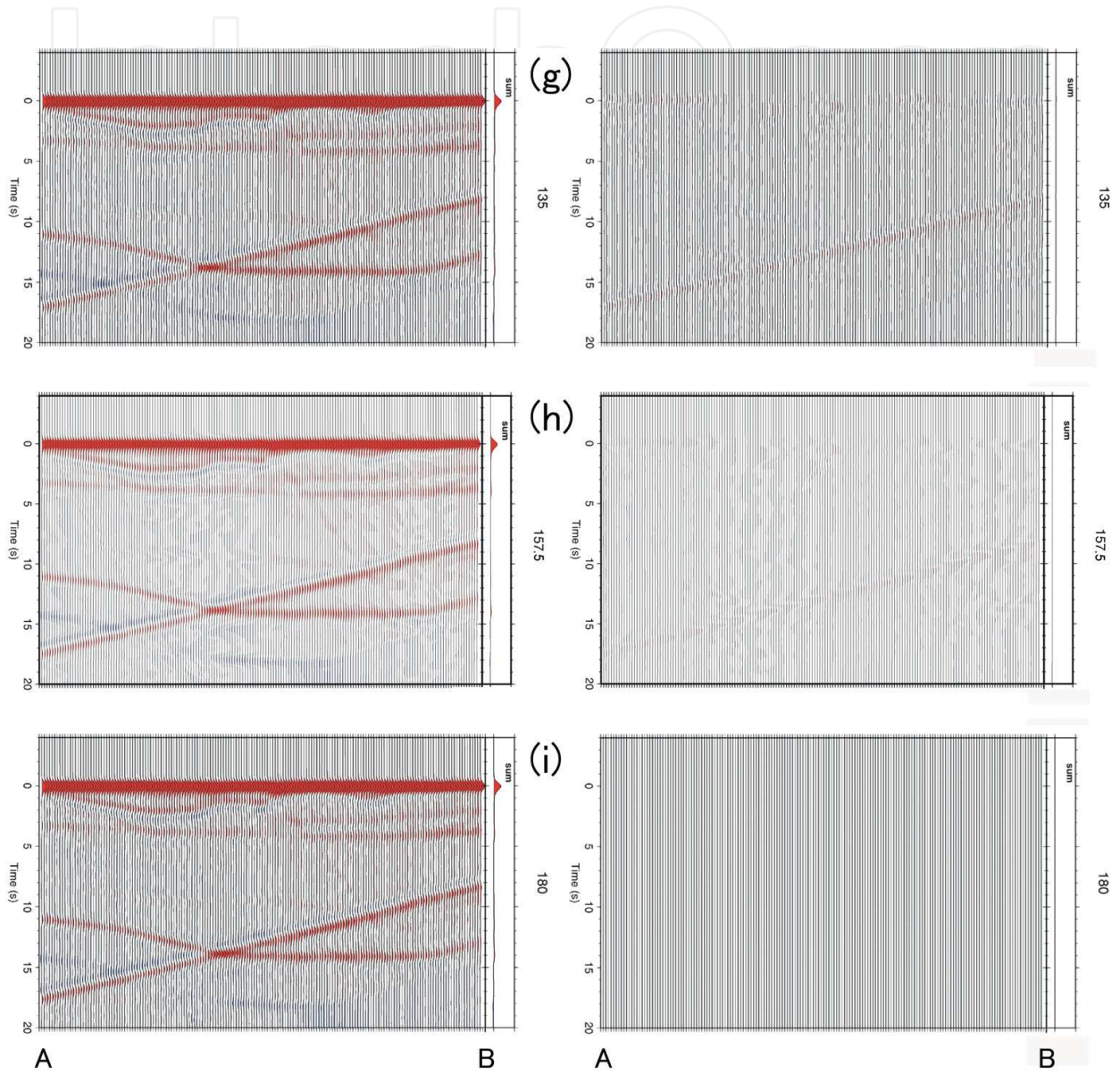
Fig. 7. **(Continued.)**

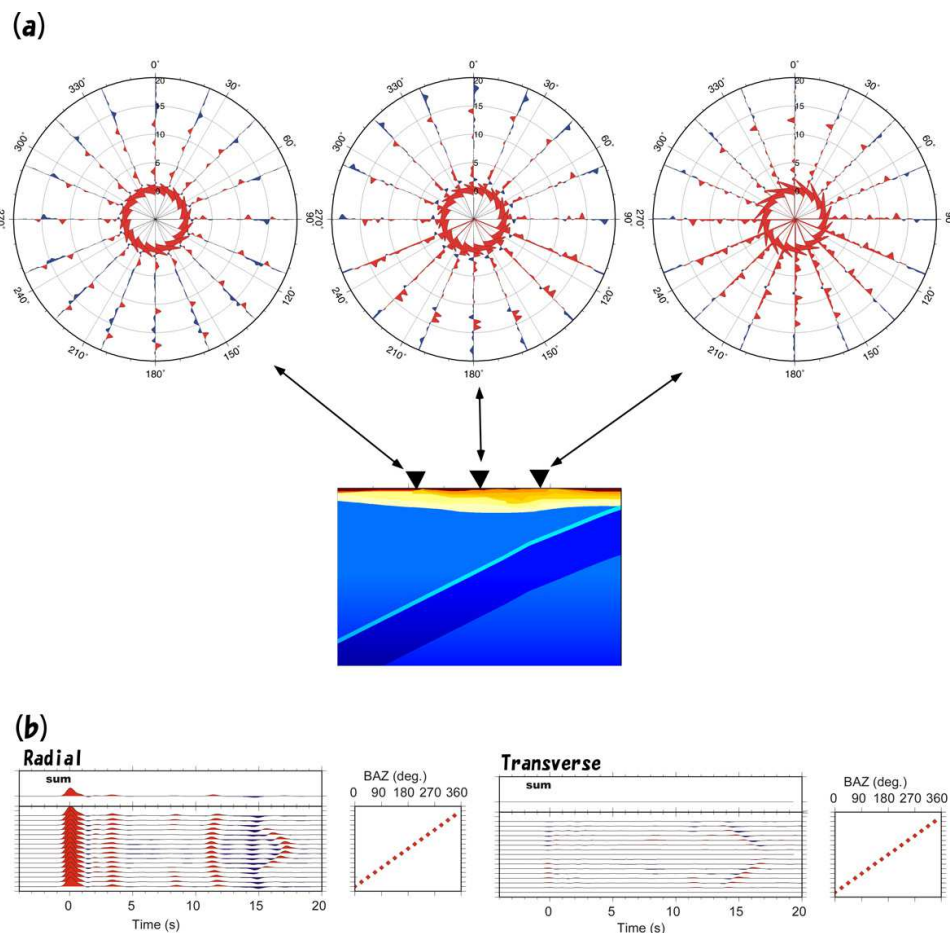Fig. 7. **(Continued.)**

(a)

(b)

Fig. 8. Receiver functions relative to backazimuth. (a) Circular plots at three stations. Delay time is plotted from −5 to 20 s from the center of the plot outward. (b) Linear plots at the left station among the three stations. Left column: radial receiver functions and their backazimuth plots, where the backazimuth of each trace is plotted at the same level as that of the trace. Right column: transverse receiver functions and their backazimuth plots.

6. Conclusion

Two-and-half-dimensional approach in the time domain has been considered for calculating three-dimensional teleseismic body wave propagation in two-dimensionally varying medium. It is an economical approach for calculating 3-D wavefields in real problems, and requires storage only slightly larger than, and computation time only slightly longer than those of the corresponding 2-D calculation. A finite-difference scheme solving the 2.5-D elastodynamic equation for 3-D seismic response of a 2-D structure model due to an obliquely incident plane wave has been described. The modelling of such seismic wavefields for a 2.5-D situation with an incident plane wave is of considerable practical importance. For instance, this approach can be applied to modelling of teleseismic body waves observed on complex crustal structures or radiated from shallow earthquakes occurring in subduction zones, where the laterally heterogeneous media can have large effects on the waveforms. We showed some numerical examples which include modelling of teleseismic body waves for the earthquake source analysis and the receiver function analysis. The method described here is very efficient, so that we expect it could be used for waveform inversions for routine-like source retrievals

and subsurface structure reconstructions from teleseismic seismograms in the near future, which need many forward modelling computations.

7. Acknowledgment

8. References

Aki, K. & Richards, P. (2002). *Quantitative Seismology (second ed.)*, University Science Books, Sausalito, California.

Ammon, C. J. (1991). The isolation of receiver effects from teleseismic *P* waveform, *Bull. Seism. Soc. Amer.* 81, 2504-2510.

Ando, T., Takenaka, H., Okamoto, T. & Murakoshi, T (2003). Modeling of receiver functions for laterally heterogeneous structures using a 2.5D FDM, *American Geophysical Union 2003 Fall Meeting, Eos Trans. AGU* 84 (46), S32A-0840, San Francisco, California, December 2003.

Bleistein, N. (1986). Two-and-one-half dimensional in-plane wave propagation, *Geophys. Prospect.* 34, 686–703.

Bouchon, M. (1976). Teleseismic body wave radiation from a seismic source in a layered medium, *Geophys. J. R. Astr. Soc.* 47, 515–530.

Cassidy, J. F. (1992). Numerical experiments in broadband receiver function analysis, *Bull. Seism. Soc. Am.* 82(3), 1453–1474.

Dugda, M. T., Nyblade, A. A., Julia, J., Langston, C. A., Ammon, C. J. & Simiyu, S. (2005). Crustal structure in EthiopiaĄ@and Kenya from receiver function analysis: Implications for rift development in eastern Africa, *J. Geophys. Res.*, 110, B01303, doi:10.1029/2004JB003065.

Dziewonski, A. M. & Anderson, D. L. (1981). Preliminary reference Earth model, *Phys. Earth Planet. Inter.* 25, 297–356.

Eskola, L. & Hongisto, H. (1981). The solution of the stationary electric field strength and potential of a point current source in a $2\frac{1}{2}$-dimensional environment, *Geophys. Prospect.* 29, 260–273.

Farra, V. & Vinnik, L. (2000). Upper mantle stratification by *P* and *S* receiver functions, *Geophys. J. Int.* 14(3), 699–712.

Furumura, T. & Takenaka, H. (1996). 2.5-D modelling of elastic waves using the pseudospectral method, *Geophys. J. Int.* 124, 820–832.

Haskell, N. A. (1953). The dispersion of surface waves in multilayered media, *Bull. Seism. Soc. Am.* 43, 17–34.

Hayashida, T., H. Takenaka, H. & Okamoto, T. (1999). Development of 2D and 3D codes of the velocity-stress staggered-grid finite-difference method for modeling seismic wave propagation, *Sci. Repts., Dept. Earth & Planet. Sci., Kyushu Univ.* 20(3), 99–110 (in Japanese with English abstract).

JafarGandomi, A. & Takenaka, H. (2007). Efficient FDTD algorithm for plane-wave simulation for vertically heterogeneous attenuative media, *Geophysics* 72(4), H43–H45.

JafarGandomi, A. & Takenaka, H. (2010). Three-component 1D viscoelastic FDM for plane-wave incidence, *Advances in Geosciences, Volume 20: Solid Earth (SE)*, edited

by Kenji Satake, World Scientific Publishing Company (ISBN-10: 981-283-817-1; ISBN-13: 978-981-283-817-9), Singapore, 299–312.

Kanao, M. & Shibutani, T. (2011). Shear wave velocity models beneath Antarctic margins inverted by genetic algorithm for teleseismic receiver functions, this book.

Kaneshima, S., T. Okamoto, T. & Takenaka, H. (2007). Evidence for a metastable olivine wedge inside the subducted Mariana slab, *Earth and Planetary Science Letters* 258(1-2), 219–227.

Kennett, B. L. N. & Engdahl, E. R. (1991). Traveltimes for global earthquake location and phase identification, *Geophys. J. Int.* 105, 429–465.

Kennett, B. L. N., Engdahl, E. R. & Buland, R. (1995). Constraints on seismic velocities in the Earth from travel times. *Geophys. J. Int.* 122, 108–124.

Kikuchi, M. & Kanamori, H. (1991). Inversion of complex body waves-III, *Bull. Seism. Soc. Am.* 81(6), 2335–2350.

Kopp, H., Klaeschen, D., Flueh, E. R. & Bialas, J. (2002). Crustal structure of the Java margin from seismic wide-angle and multichannel reflection data, *J. Geophys. Res.* 107, doi:10.1029/2000JB000095.

Kroeger, G. C. & Geller, R. J. (1983). An efficient method for computing synthetic reflections for plane layered models, *EOS Trans. AGU* 64, 772.

Langston, C. A. (1977). The effect of the planar dipping structure on source and receiver responses for constant ray parameter, *Bull. Seism. Soc. Am.* 67, 1029–1050.

Langston, C. A. (1979). Structure under Mount Rainier, Washington, inferred from teleseismic body waves, *J. Geophys. Res.* 84, 4749–4762.

Laske, G., Masters, G. & Reif, C. (2001). CRUST 2.0: A new global crustal model at 2×2 degrees, `http://mahi.ucsd.edu/Gabi/rem.html`.

Levander, A.R. (1988). Fourth-order finite-difference *P-SV* seismograms, *Geophysics* 53, 1425–1436.

Luco, J.E., Wong, H.L. & De Barros, F.C.P. (1990). Three-dimensional response of a cylindrical canyon in a layered half-space, *Earthquake Eng. Struct. Dyn.* 19, 799–817.

Miyamura, J. & Sasatani, T. (1986). Accurate determination of source depths and focal mechanisms of shallow earthquakes occurring at the junction between the Kurile and the Japan trenches *Journal of the Faculty of Science, Hokkaido University. Series 7, Geophysics* 8(1), 37–63.
`http://hdl.handle.net/2115/8752`

Nakamura, T., Tsuboi, S., Kaneda, Y. & Yamanaka, Y. (2009). Rupture process of the 2008 Wenchuan, China earthquake inferred from teleseismic waveform inversion and forward modeling of broadband seismic waves, *Tectonophysics* 491(1–4), 72–84, doi 10.1016/j.tecto.2009.09.020.

Okamoto, T. (1993). Effects of sedimentary structure and bathymetry near the source on teleseismic *P* waveforms from shallow subduction zone earthquakes, *Geophys. J. Int.* 112, 471–480.

Okamoto, T. (1994). Teleseismic synthetics obtained from 3-D calculations in 2-D media, *Geophys. J. Int.* 118, 613–622.

Okamoto, T. & Miyatake, T. (1989). Effects of near source seafloor topography on long-period teleseismic *P* waveforms, *Geophys. Res. Lett.* 16, 1309–1312.

Okamoto, T. & Takenaka, H. (2009a). Waveform inversion for slip distribution of the 2006 Java tsunami earthquake by using 2.5D finite-difference Green's function, *Earth Planets*

Space 61(5), e17–e20.
http://www.terrapub.co.jp/journals/EPS/pdf/2009e/6105e017.pdf

Okamoto, T. & Takenaka, H. (2009b). Effect of near-source trench structure on teleseismic body waveforms: an application of a 2.5D FDM to the Java Trench, *Advances in Geosciences, Volume 13: Solid Earth (SE)*, edited by Kenji Satake, World Scientific Publishing Company, Singapore (ISBN-10: 981-283-617-9; ISBN-13: 978-981-283-617-5), 215–229.

Okamoto, T., Takenaka, H., Nakamura, T. & Aoki, T. (2010). Accelerating large-scale simulation of seismic wave propagation by multi-GPUs and three-dimensional domain decomposition, *Earth Planets Space* 62(12), 939–942.
http://www.terrapub.co.jp/journals/EPS/abstract/6212/62120939.html

Owens, T. J., Crosson, R. S. & Hendrickson, M. A. (1988). Constraints on the subduction geometry beneath western Washington from broadband teleseismic waveform modeling, *Bull. Seism. Soc. Am.* 78(3), 1319–1334.

Pedersen, H.A., Sánchez-Sesma, F.J. & Campillo M. (1994). Three-dimensional scattering by two-dimensional topographies, *Bull. seism. Soc. Am.* 84, 1169–1183.

Randall, C.J. (1991). Multipole acoustic waveforms in nonaxisymmetric boreholes and formations, *J. Acoust Soc. Am.* 90, 1620–1631.

Saita, T., Suetsugu, D., Ohtaki, T., Takenaka, H., Kanjo, K. & Purwana, I. (2002). Transition zone thickness beneath Indonesia as inferred using the receiver function method for data from the JISNET regional broadband seismic network, *Geophys. Res. Lett.* 29(7), doi:10.1029/2001GL013629.

Suetsugu, D., Saita, T., Takenaka, H. & Niu, F. (2004). Thickness of the mantle transition zone beneath the South Pacific as inferred from analyses of ScS reverberated and Ps converted waves, *Phys. Earth Planet. Inter.* 146, 35–46, doi:10.1016/j.pepi.2003.06.008.

Takenaka, H. & B.L.N. Kennett (1996a). A 2.5-D time-domain elastodynamic equation for plane-wave incidence, *Geophys. J. Int.* 125, F5–F9.

Takenaka, H. & B.L.N. Kennett (1996b). A 2.5-D time-domain elastodynamic equation for a general anisotropic medium, *Geophys. J. Int.* 127, F1–F4.

Takenaka, H., Kennett, B.L.N., & Fujiwara, H. (1996). Effect of 2-D topography on the 3-D seismic wavefield using a 2.5-D discrete wavenumber - boundary integral equation method, *Geophys. J. Int.* 124, 741–755.

Takenaka, H. & Okamoto, T. (1997). Teleseismic waveform synthesis for ocean-bottom stations using a new, very effective 2.5-D finite difference technique, *Proceedings of International Workshop on Scientific Use of Submarine Cables*, pp. 23–26, Okinawa, Japan, February 1997.

Takenaka, H., Okamoto, T. & Kennett, B. L. N. (1997). A very effective 2.5-D method for teleseismic body-wave synthesis, *Programme and Abstracts, The Seismological Society of Japan 1997, No.2*, B65 (in Japanese), Hirosaki, Japan, September 1997.

Takenaka, H., Ando, T. & Okamoto, T. (2004). Investigation on azimuthal dependence of slab-converted phases observed in receiver functions by 2.5-D numerical simulations, *Abstracts 2004 Japan Earth and Planetary Science Joint Meeting*, I021-002, Chiba, May 2004.

Tanaka, H. & Takenaka, H. (2005). An efficient FDTD solution for plane-wave response of vertically heterogeneous media, *Zisin (Journal of the Seismological Society of Japan)* 57(3), 343–354 (in Japanese with English abstract).

```
http://www.journalarchive.jst.go.jp/english/jnltop_en.php?
cdjournal=zisin1948
```

Thomson, W. T. (1950). Transmission of elastic waves through the stratified solid medium, *J. Appl. Phys.* 21, 89–93.

Virieux, J. (1986). *P-SV* wave propagation in heterogeneous media: Velocity-stress finite-difference method, *Geophysics* 51, 889–901.

Wiens, D. A. (1987). Effects of near source bathymetry on teleseismic *P* waveforms, *Geophys. Res. Lett.* 14, 761–764.

Wiens, D. A. (1989). Bathymetric effects on body waveforms from shallow subduction zone earthquakes and application to seismic processes in the Kurile trench, *J. Geophys. Res.* 94, 2955–2972.

Yoshida, S. (1992). Waveform inversion for rupture process using a non-flat seafloor model: application to 1986 Andreanof islands and 1985 Chile earthquakes, *Tectonophysics* 211,45–59.

Zhu, L. & Kanamori, H. (2000). Moho depth variation in southern California from teleseismic receiver functions, *J. Geophys. Res.* 105, 2969–2980.
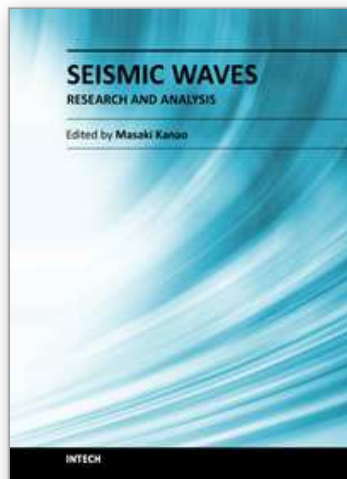
Seismic Waves - Research and Analysis

Edited by Dr. Masaki Kanao

The importance of seismic wave research lies not only in our ability to understand and predict earthquakes and tsunamis, it also reveals information on the Earth's composition and features in much the same way as it led to the discovery of Mohorovicic's discontinuity. As our theoretical understanding of the physics behind seismic waves has grown, physical and numerical modeling have greatly advanced and now augment applied seismology for better prediction and engineering practices. This has led to some novel applications such as using artificially-induced shocks for exploration of the Earth's subsurface and seismic stimulation for increasing the productivity of oil wells. This book demonstrates the latest techniques and advances in seismic wave analysis from theoretical approach, data acquisition and interpretation, to analyses and numerical simulations, as well as research applications. A review process was conducted in cooperation with sincere support by Drs. Hiroshi Takenaka, Yoshio Murai, Jun Matsushima, and Genti Toyokuni.

INTECH
open science | open minds